J. Am. Ceram. Soc., 80 [3] 637–45 (1997)

Sintering of Fine Oxide Powders: II, Sintering Mechanisms

Pei-Lin Chen* and I-Wei Chen*

Materials Sciences and Engineering, University of Michigan, Ann Arbor, Michigan 48109

Conventional and new sintering mechanisms have been investigated using fine powders of CeO_2 and Y_2O_3 of excellent sinterability. We have verified the validity of Herring's scaling law for 60%–84% relative density and found that it is consistent with grain-boundary-diffusion control. At lower densities, we have found that pores larger than the critical size, in the sense of Kingery and Francois, can still be sintered readily. This is rationalized by a new sintering mechanism based on particle repacking concurrent with particle coarsening, resulting in a higher packing factor. Very fine, surface-active powders that coarsen rapidly are uniquely capable of taking advantage of this new sintering mechanism, which along with their propensity to homogenization, accounts for their remarkable sinterability even at very low green densities.

I. Introduction

In the previous paper (hereafter referred to as Paper I),[1] we have shown that obtaining fine CeO_2 and Y_2O_3 powders using high-yield precipitation methods is possible and that dry-pressed compacts could be sintered to full density at temperatures as low as 45% of their respective melting points. The excellent sinterability was further demonstrated with some very-low-green-density (18%) bodies that were subsequently fired to full density. The pore-size distributions of powder compacts, when normalized by the particle size, evolved during firing in an essentially universal manner, dependent on the density, but otherwise independent of material type, powder size, and prior history of either packing or firing. The normalized pore size can be quantitatively described by a network model that assumes a random, yet spatially homogeneous, distribution of spherical particles. In the initial stage of firing, homogenization of the microstructure was, indeed, observed, as reflected by the sharpening of the pore-size distribution, sometimes with minimal or no concurrent densification. Another evolution toward homogenization was observed in the final stage of sintering after full density had been achieved. With a gradual increase in the grain size, the grain-shape distribution sharpens to form five-sided grains on planar cross sections. Because all these features are consistent with a uniform packing and uniform microstructure at all densities, the excellent sinterability of these fine powders can be attributed to their ability to attain such uniformity, regardless of the method and the density used in the initial packing.

One obvious feature that distinguishes the sintering of fine powders from that of coarser powders is the strong tendency for particle coarsening during firing. Particle coarsening in very porous compacts is well-known in the ceramic literature.[2–6] However, several reports have been presented recently that show that particle/grain size can remain essentially constant up to a density of ~92%, and such a resistance to coarsening has been claimed to be essential for good sinterability because it signifies uniform packing.[7,8] These observations also have reinforced the notion that sinterability reflects the competition between densification and coarsening and that coarsening is detrimental to good sinterability.[9] However, in our study of fine CeO_2 and Y_2O_3 powders, we have found good sinterability, regardless of coarsening behavior.[1] Specifically, CeO_2 coarsened more than Y_2O_3 at comparable temperatures and densities; yet, compacts of both oxides could be readily sintered to full density. Coarsening was further found to begin at very early stages, in all cases $\ll$92%. These observations with fine powders clearly contradict the popular notion of an inverse correlation between sinterability and coarsening. Because this strong tendency for coarsening could very well be an inherent part of the "activity" of very fine, highly sinterable powders, its role is worth further scrutiny in the context of fundamental concepts in the sintering theory.

In the present paper, we explore, in detail, the role of particle coarsening in various stages of sintering. At higher densities, we examine the applicability of Herring's scaling law, which, by stating the particle-size effect on diffusion-controlled kinetics, forms the basis of the promise of fine powders.[10] At lower densities, because we have determined the critical pore size, in the sense of Kingery and Francois,[11] in Paper I, we are in a position to assess the driving force and, hence, the sinterability of the larger pores. We find, surprisingly, that supercritical pores do shrink in the compacts of fine powders irrespective of their thermodynamic disadvantage, which prompts us to propose a new coarsening-motivated repacking mechanism to explain their unexpected shrinkage. Lastly, we will elaborate on our previous observation of microstructure homogenization and relate it to coarsening and to packing modification at very low densities. Together, these concepts will provide a comprehensive framework for understanding the sintering kinetics of fine powder compacts at various stages.

All the experimental procedures used in the present work have been described in Paper I. Indeed, we will extensively refer to the experimental data reported in Paper I for our analysis. We also will follow the notation for symbols used therein. In the following, we will first present the sintering curves, as a function of temperature and the particle size, to highlight the role of particle coarsening. These results are then analyzed using sintering models.

II. Sintering Curves

Sintering curves of Y_2O_3 at a constant heating rate are shown in Fig. 1, to demonstrate the effect of initial particle size. Powder Y(E), which has an initial particle size of 13 nm, began to sinter at a temperature several hundred degrees lower than the coarser powders. The largest difference is seen at 70%, which is achieved at 840°C in powder Y(E) and at 1400°C in powder Y(A) (initial particle size = 230 nm). The shape of the sintering curves also is different for different powders. For finer powders—Y(D) and Y(E)—an inflection point in the curve is

J. E. Blendell—contributing editor

Manuscript No. 192213. Received November 3, 1995; approved September 17, 1996.

Supported by the U.S. Department of Energy under Grant No. DE-FG02-87ER45302.

Presented at the 97th Annual Meeting of the American Ceramic Society, Cincinnati, OH, May, 1995 (Science, Technology and Commercialization of Powder Synthesis and Shape Forming Process Symposium, Paper No. SXIX 04-95).

*Member, American Ceramic Society.

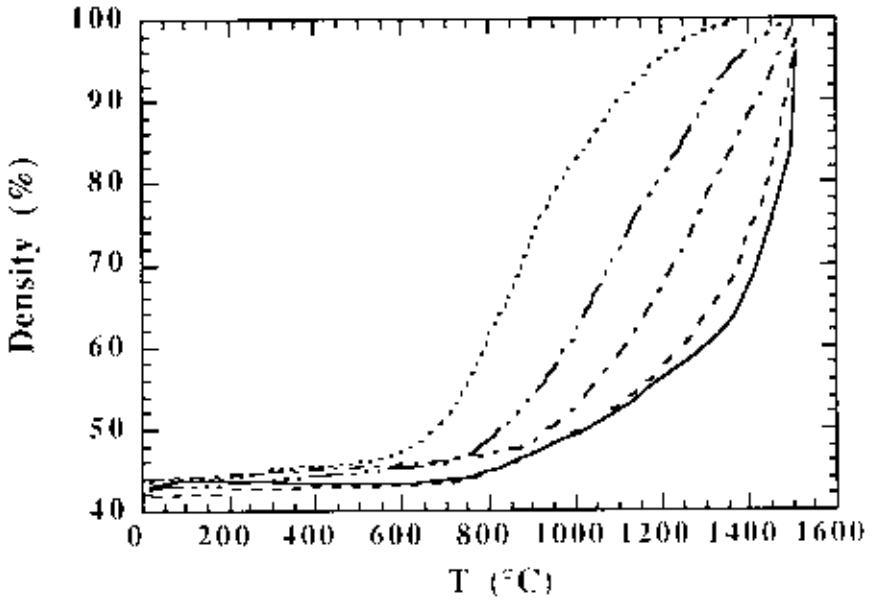

Fig. 1. Sintering curves of Y_2O_3 powders ((—) Y(A), particle size of 230 nm; (– – –) Y(B), particle size of 145 nm; (–·–) Y(C), particle size of 32 nm; (–···–) Y(D), particle size of 21 nm; and (···) Y(E), particle size of 13 nm).

present that is not found for coarser powders Y(A), Y(B), and Y(C).

Sintering curves of CeO_2 are shown in Fig. 2, covering a range of initial particle sizes (69 nm for Ce(A) and 16 nm for Ce(B)). The green density of the compacts varies from 20%–50% in this study. Again, starting with the same green density, coarser powders require a higher temperature to sinter (compare the two powders at 41%). For the same powder, a higher green density seems to lower the sintering temperature. In all cases, an inflection in the sintering curve is seen at ~65%.

The abovementioned sintering curves, in the form of density versus temperature, mask the influence of particle coarsening that occurred as temperature increased. As shown in Paper I, under a constant heating rate, the particle size is a function of temperature, essentially independent of density. These data are shown again in Fig. 3 for reference. Note that, at low temperatures, CeO_2 powders coarsen more rapidly. Using these data, the densification curves can be replotted as a function of particle size instead of temperature, shown in Fig. 4. We may picture these curves to have a characteristic S shape, which is better developed for Ce(B) compacts that coarsen readily. The S-shaped curve contains a constant density region at small particle sizes, an intermediate region with a steep increase of density from 40% to 60%, and a third region at large particle sizes with a slower increase in density. These characteristic curves can be normalized if we rescale the particle size by its value at, for example, 50% density. Using this procedure, we have replotted all the data (except Y(A), which did not coarsen much, according to Fig. 3) in Fig. 5. Then, all the curves clearly fall onto each other in the middle region, where density

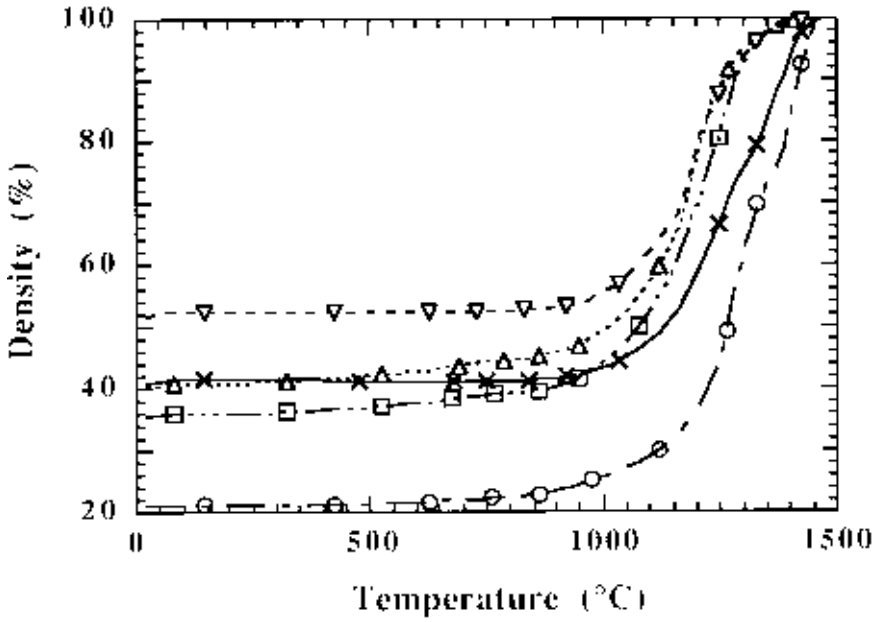

Fig. 2. Sintering curves of CeO_2 powders ((×) Ce(A), 41% green density, particle size of 67 nm; (▽) Ce(A), 51% green density, particle size of 67 nm; (○) Ce(B), 21% green density, particle size of 16 nm; (□) Ce(B), 36% green density, particle size of 16 nm; and (△) Ce(B), 41% green density, particle size of 16 nm).

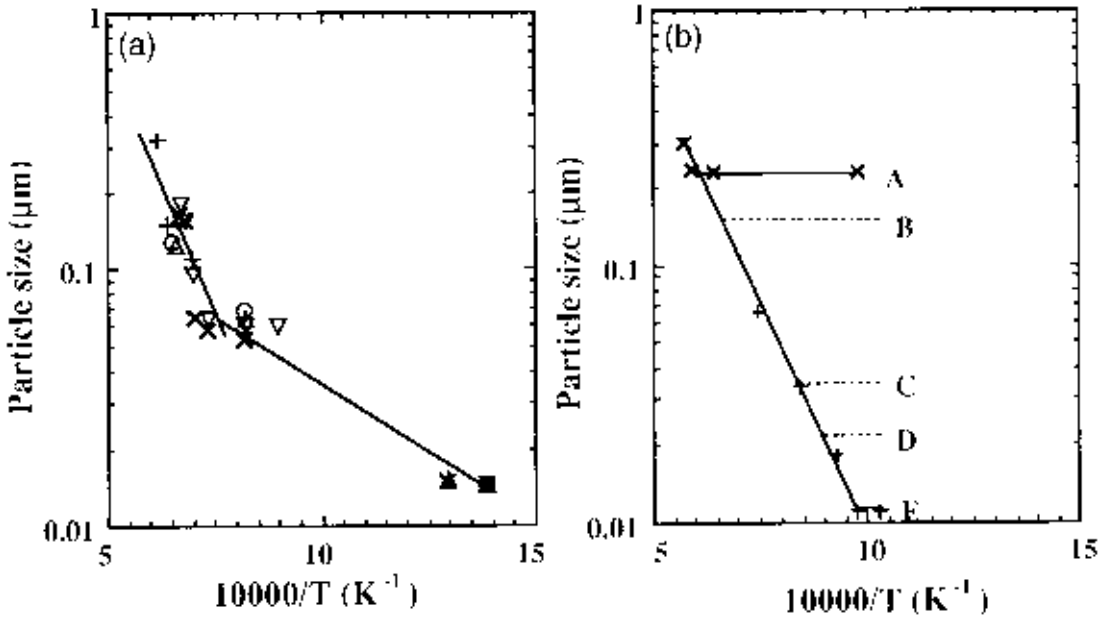

Fig. 3. Particle sizes during sintering interrupted at different temperatures for (a) CeO_2 ((▽) Ce(A) with 51% green density and Ce(B) with (○) 21%, (+) 27%, (△) 36%, and (×) 41% green density) and (b) Y_2O_3 ((×) Y(A) with 44% green density and (+) Y(E) with 43% green density; initial particle sizes for Y(B), Y(C), and Y(D) are indicated by dotted lines).

increases steeply. Notably, the actual choice of the reference value of particle size is not important, because essentially similar plots can be obtained by choosing the reference value at any density in the range of 40%–60%.

III. Sintering Mechanisms

(1) Coarsening-Motivated Packing (Region II)

We first focus on the middle region (region II) in Fig. 5. In this region, the density increases from 40% to 65%. As shown in Paper I, the critical ratio of pore size to particle size, in the sense of Kingery and Francois,[11] was determined to be 0.38 for CeO_2 and Y_2O_3. Using this value, a reexamination of the normalized pore size data in Paper I reveals an important discrepancy between the data and the conventional theory of solid-state sintering.[11] For example, in Figs. 10(a)–(d) of Paper I, almost all the pores are initially supercritical; yet, they apparently shrink and the overall density of the compacts increases. Specifically, we note that, in Fig. 10(a) of Paper I, a large increase in density, from 29% to 66%, occurs even though the normalized pore size is still supercritical at 66%. The same also is observed for the density increase from 41% to 62% in Fig. 10(b) of Paper I, from 51% to 62% in Fig. 10(c) of Paper I, and probably also from 48% to 60% in Fig. 10(d) of Paper I. (Only in Fig. 10(e) of Paper I is a substantial portion of the initial r/R value <0.38 and, hence, subcritical.) Indeed, because CeO_2 powder compacts of a density as low as 18%, which had

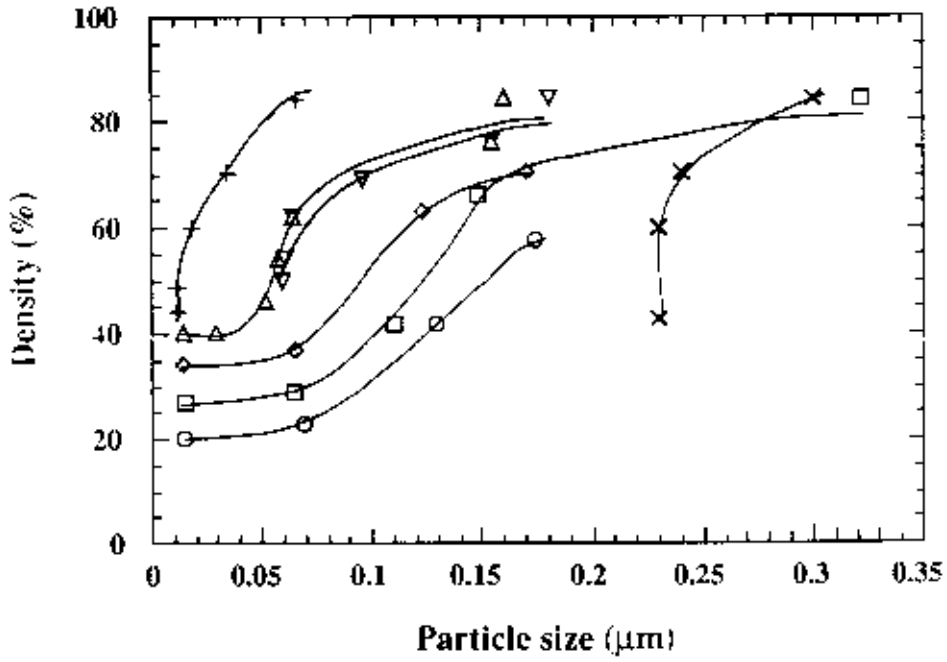

Fig. 4. Densification curves, as a function of particle size ((▽) Ce(A) with 51% green density; Ce(B) with (○) 20.6%, (□) 26.8%, (◇) 35.8%, and (△) 41% green density; (×) Y(A) with 44% green density; and (+) Y(E) with 43% green density).

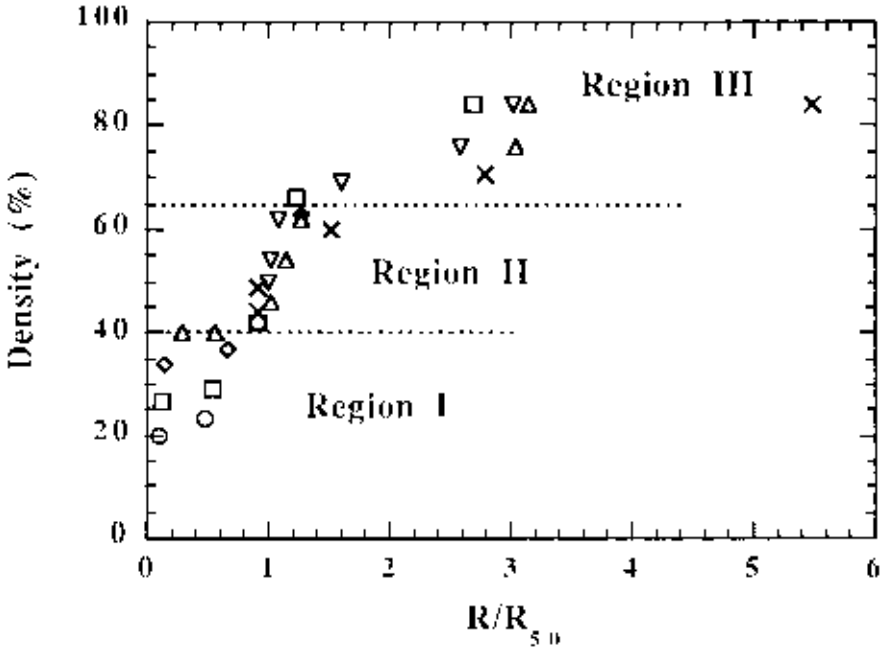

Fig. 5. Densification curves, as a function of normalized particle size ((▽) Ce(A) with 51% green density; Ce(B) with (○) 20.6%, (□) 26.8%, (◇) 35.8%, and (△) 41% green density; and (×) Y(E) with 43% green density). R_{50} is the particle size at 50% density.

an even larger ratio of r/R, according to Fig. 11 of Paper I, could be readily sintered to full density in our study, they strongly argue for a new pore shrinkage and densification mechanism that is not based on the concept of critical pore size. This mechanism is most relevant for region II in Fig. 5 that covers the intermediate density.

The mechanism we propose is based on an extension of our packing model[1] by incorporating particle coarsening. Specifically, we assume that mass is locally preserved and that particle contacts are maintained, whereas packing evolves with particle coarsening. As schematically illustrated in Fig. 6, coarsening of particles under these assumptions leads to a decrease of pore volume and an increase of packing density. This involves a coordinated inward movement of coarsened particles on a "ring" (see Fig. 6) toward the central pore, to maintain particle contacts. As the extra pore space is displaced to the exterior of the ring, a compact full of such particle rings shrinks macroscopically. This packing mechanism fundamentally differs from the conventional densification mechanism in solid-state sintering in that vacancy transport out of pores via grain-boundary or lattice diffusion is not explicitly required.[12] Therefore, it does not hinge on the concept of critical pore size, which has been used to determine the thermodynamic driving force and, hence, the direction of vacancy fluxes.[11] Nevertheless, capillarity is still the reason for maintaining the particle–particle contacts during coarsening and, hence, the cause for the coordinated inward movement of particles during repacking. In reality, some rotation or interparticle sliding is likely to be involved in the repacking process envisioned in Fig. 6, and some grain-boundary migration following surface diffusion is likely to be involved in the coarsening process, as envisioned by Greskovich and Lay.[3] To this extent, therefore, some grain-boundary diffusion is probably necessary. For simplicity, however, we will ignore the latter aspects and focus on the concept of coarsening and repacking depicted in Fig. 6 to evaluate the contribution and kinetics of this new mechanism.

We start with mass conservation and state that the total volume of particles on the ring surrounding a pore remains the same during coarsening and repacking:

$$nR^3 = \text{constant} = C_1 \tag{1}$$

Here, n is the number of spherical particles (of radius R) on the ring surrounding a pore (of radius r). According to the packing model of Egami and Aur,[13] n can be expressed in terms of r/R:

$$n = \frac{4\pi\left[1 - \left(\frac{3}{4}\right)^{1/2}\right]}{1 - \frac{\left[\frac{r}{R}\left(\frac{r}{R} + 2\right)\right]^{1/2}}{\frac{r}{R} + 1}} \tag{2}$$

The above expression has been verified by computer simulation of binary metallic glasses over the range of $0 < r/R < 1$ and is in agreement with the polyhedron model in the same range. It also has the appropriate asymptotic form: $n = C_2(r/R)^2$ in the limit of $r/R \gg 1$, with $C_2 = 3.4$. Substituting this equation and the density (ρ)–r/R correlation of Paper I,

$$\frac{1 - \rho}{\rho} = \frac{r}{R} \tag{3}$$

into Eq. (1), we obtain

$$\left(\frac{R}{R_0}\right)^3 = 1 - (1 - \rho^2)^{1/2} \tag{4}$$

where R_0 is a normalization constant that is related to C_1 and the numerator of Eq. (2). Note that, at $\rho = 0.5$, $R/R_0 = 0.51$. Thus, R_0 can be conveniently approximated as twice the particle size at $\rho \approx 0.5$, i.e., $R_0 = 2R_{50}$ in Fig. 5. This relation is plotted in Fig. 7, for comparison with the data in Fig. 5. For later reference, we also have obtained n vs ρ in the following equation from Eqs. (2) and (3):

$$n = \frac{4\pi\left[1 - \left(\frac{3}{4}\right)^{1/2}\right]}{1 - (1 - \rho^2)^{1/2}} \tag{5}$$

which increases as ρ decreases.

The shape of the R–ρ curve predicted by Eq. (4) compares well with the experimental data that fall into region II. At lower density, although the samples show very little densification despite considerable coarsening and, hence, cannot be described by Eq. (4), we find the upper envelope of each family of data in region I falls on the predicted curve. Thus, once coarsening has caused certain microstructural changes (see Section III*(3)*), the densification can be described by Eq. (4) at a ρ value as low as

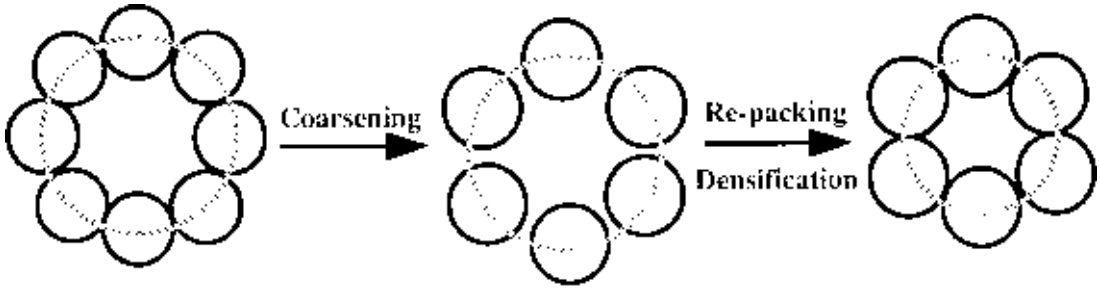

Fig. 6. Particle coarsening and repacking in region II. Note that particle contacts are maintained and mass is conserved, whereas the pore space decreases and the packing factor increases.

0.25. At $\rho > 0.65$, we do not expect the present mechanism to be applicable; particle repacking is not feasible, because the compact becomes closely packed. (For random close packing, $\rho_{rcp} = 0.63$.[1]) Moreover, according to Fig. 11(a) of Paper I, pores at $\rho > \rho_{rcp}$ have a r/R ratio of <0.3 and are essentially subcritical. Thus, the conventional sintering mechanism will most likely intervene at $\rho > \rho_{rcp}$, causing the density to evolve differently (see Section III*(2)*).

The rate equation for sintering by coarsening-motivated repacking follows directly from Eq. (4) by differentiation with respect to time. After rearrangement, we obtain

$$\frac{d\rho}{dt} = 3f(\rho)\frac{1}{R}\frac{dR}{dt} \tag{6}$$

where $f(\rho) = [(1 - \rho^2)^{1/2} - (1 - \rho^2)]/\rho$. It reduces to zero at $\rho = 0$ and $\rho = 1$, but increases monotonically up to $\rho = 0.79$. Thus, this new mechanism is most important in the region of the intermediate density up to ρ_{rcp}, and the sintering rate is now related to the coarsening rate of the particles. Assuming the coarsening rate follows the relation

$$\frac{dR}{dt} = A\frac{D_s\gamma_s}{R^3} \tag{7}$$

as suggested by Greskovich and Lay,[3] where A is a proportionality constant, D_s the surface diffusivity, and γ_s the surface energy, we expect the sintering rate due to the above mechanism to follow a form of modified Herring's law:

$$\frac{d\rho}{dt} = \frac{\tilde{f}(\rho)}{kTR^m}D_0 \exp\left(-\frac{Q}{kT}\right) \tag{8}$$

In the above equation, $\tilde{f}(\rho) = Af(\rho)$ and $m = 4$; T is temperature, k is Boltzmann's constant, and the effective diffusivity (with a prefactor D_0 and an activation energy Q) is that of surface diffusion.

The activation energy of surface diffusion may be estimated from Fig. 3, which should essentially follow $R^4 \propto D_s$, under the constant-heating-rate condition. This gives activation energies of 2.7 and 4.4 eV, respectively, for Y_2O_3 and CeO_2. Such values are ~70% of the activation energy of grain-boundary mobility in Y_2O_3 (4.1 eV)[14] and CeO_2 (6.0 eV),[15] which seems quite reasonable. To compare the activation energy of coarsening with that of densification, we have calculated the densification rate from the slope of the sintering curve multiplied by the heating rate. We then plot the CeO_2 data, TR^4 ($d\rho/dT$), at a constant density, $\rho = 0.53$. (Thus, $f(\rho) =$ constant in Eq. (8).) As obtained from the slope of Fig. 8, the activation energy for densification rate is 4.6 eV, which is quite similar to that of coarsening. Therefore, the model presented above seems to be self-consistent.

(2) Conventional Solid-State Sintering (Region III)

The densification data in region III are analyzed assuming a conventional sintering mechanism governed by either lattice diffusion or grain-boundary diffusion. The rate equation for these mechanisms is generally written in the form of the modified Herring's law—Eq. (8)—where the exponent m is 3 for

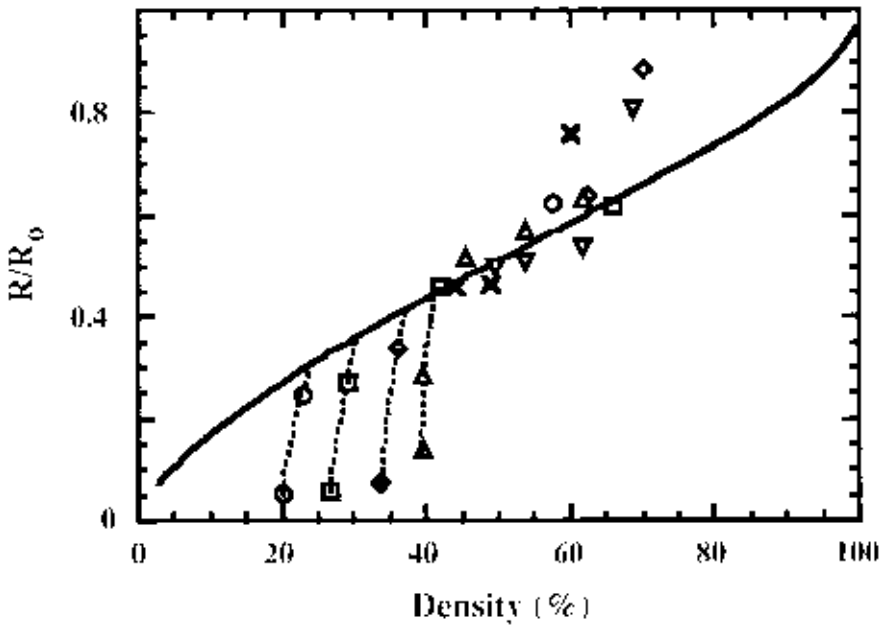

Fig. 7. Comparison between prediction of the coarsening model and the measured ratio R/R_0 ((—) calculated from Eq. (4); (▽) Ce(A) with 51% green density; Ce(B) with (○) 20.6%, (□) 26.8%, (◇) 35.8%, and (△) 41% green density; and (×) Y(E) with 43% green density).

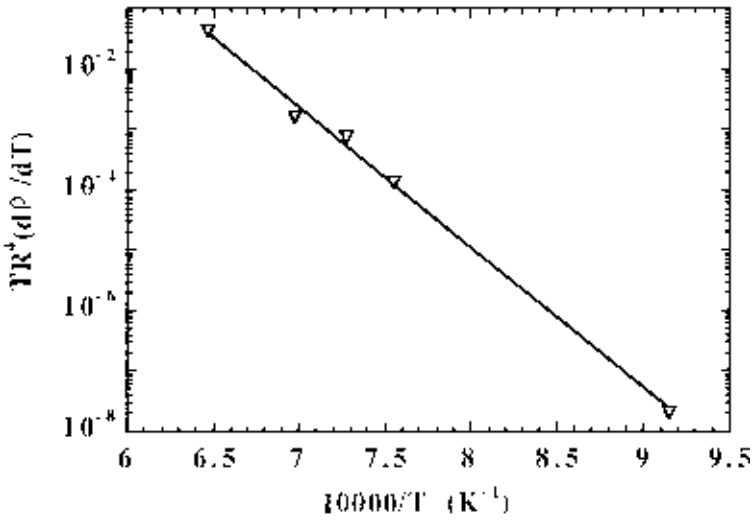

Fig. 8. Size-compensated densification rate versus reciprocal temperature, with $m = 4$ for CeO_2. Region II at $\rho = 0.53$.

lattice-diffusion control and 4 for grain-boundary-diffusion control, and $D_0 \exp[-Q/(kT)]$ is similarly identified with these diffusion mechanisms. To fit this equation, the densification rate is calculated from the slope of the sintering curve multiplied by the heating rate. We then plot TR^m $(d\rho/dt)$ against reciprocal temperature $(1/T)$ at a given density ρ, using the particle-size data in Fig. 3. This procedure is followed for three densities—60%, 70%, and 84%—for each of the Y_2O_3 and CeO_2 powders. As shown in Fig. 9, a straight-line fit of all the Y_2O_3 data can be obtained by assuming $m = 4$. The activation energy implied by this plot is 3.5 eV, which may be identified with the activation energy of grain-boundary diffusion. Note that the data for different densities in Fig. 2 fall on the same trend line, suggesting that $f(\rho)$ is almost independent of ρ in the range of 60%–84% shown here. This finding is in agreement with the calculations by Hansen *et al.*,[16] who found, for ρ values ranging from 60%–90%, $f(\rho)$ remains almost constant for grain-boundary and volume diffusion, despite the change of pore–particle geometry between what are commonly called the initial, intermediate, and final stages of sintering. A similar observation is made for all the CeO_2 data, which are shown in Fig. 10. The activation energy (presumably for grain-boundary diffusion) is 5.5 eV.

Accepting $f(\rho)$ as a constant, independent of density, Figs. 9 and 10 do not uniquely determine m nor does the sintering mechanism by itself. This is because the particle size also follows an Arrhenius behavior, as shown in Fig. 3. This ambiguity is illustrated by replotting the Y_2O_3 data using $m = 3$, shown in Fig. 11, in which an equally good straight-line Arrhenius correlation also is obtained. This plot gives an activation energy of 2.4 eV, which may be identified with lattice diffusion. However, because the grain-boundary mobility of undoped Y_2O_3 in the temperature range of 1500°–1650°C has an activation energy of 4.1 eV,[14] the much lower activation energy inferred here for lattice diffusion is unreasonable, and this interpretation must be rejected. In comparison, the activation energy of 3.5 eV in Fig. 9 seems reasonable in the same context. Thus, we conclude that only $m = 4$ is acceptable and that sintering in this density regime is consistent with grain-boundary-diffusion control. Similarly, we have constructed a similar plot for CeO_2 data using $m = 3$, as shown in Fig. 12. Although the fit is again satisfactory, the implied lattice diffusion has an activation energy of 4.0 eV, which is smaller than that of the grain-boundary mobility of undoped CeO_2—6.0 eV.[15] Again, this seems unreasonable, and the interpretation should be rejected.

(3) Nondensifying Coarsening (Region I)

At low densities, particles coarsen with relatively little densification as can be seen in region I of Fig. 5. As discussed in Paper I, although the overall density in region I barely changes, some very large pores tend to disappear, which is attributed to stochastic particle relocation leading to pore-volume redistribution. The cause of particle relocation, after the initial firing transient, is suggested to be also related to coarsening, because interparticle contacts must be repeatedly perturbed by surface diffusion and movement of grain boundary,[3] which leaves noncentral interparticle forces that motivate particle sliding and rotation. The reason very little densification on a macroscopic scale occurs frequently at this stage, we believe, is the relatively low connectivity in the particle network at low densities. According to Eq. (3) and Fig. 15 in Paper I, at $\rho = 0.25$, for example, each particle is typically in contact with approximately three other particles. Meanwhile, at the same density, a typical pore has a size $3R$, according to Eq. (3), and tens of surrounding particles. In such a microstructure, any disruption of the particle connections, which is likely in any real packing and also has been observed in various desintering models

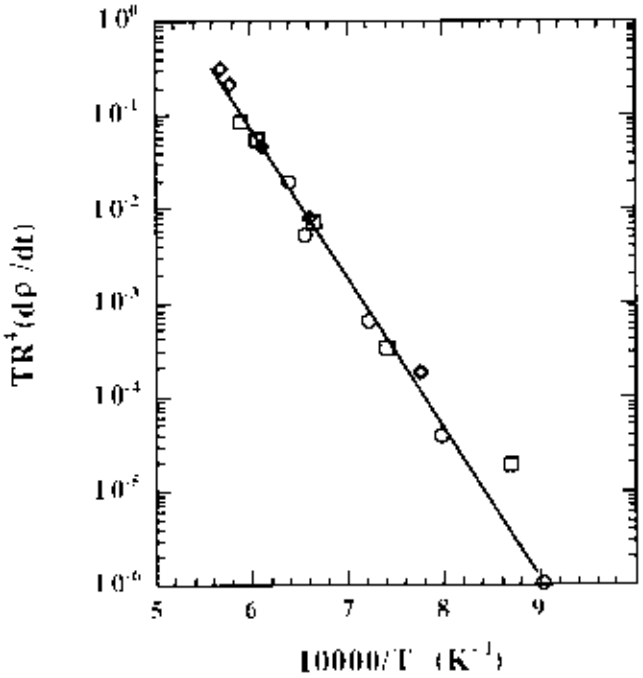

Fig. 9. Size-compensated densification rate versus reciprocal temperature, with $m = 4$, for Y_2O_3 at various densities ((○) 60%, (□) 70%, and (◇) 84%).

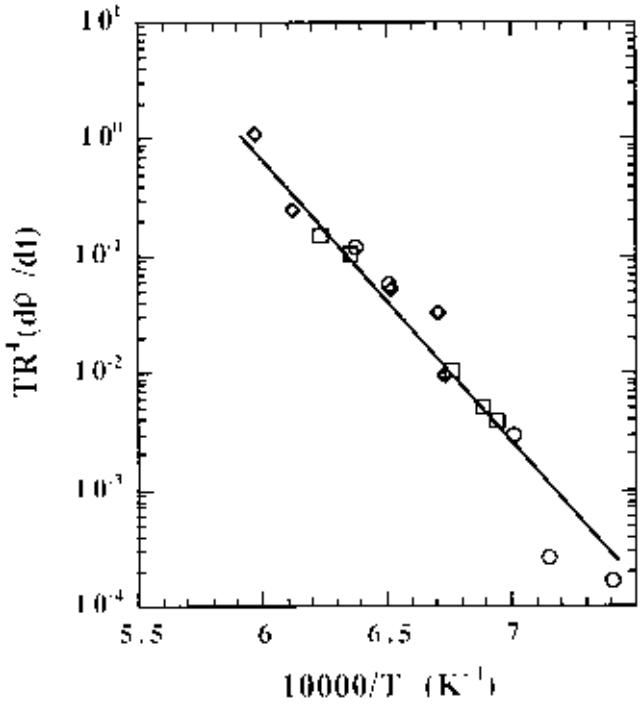

Fig. 10. Size-compensated densification rate versus reciprocal temperature, with $m = 4$, for CeO_2 at various densities ((○) 60%, (□) 70%, and (◇) 84%).

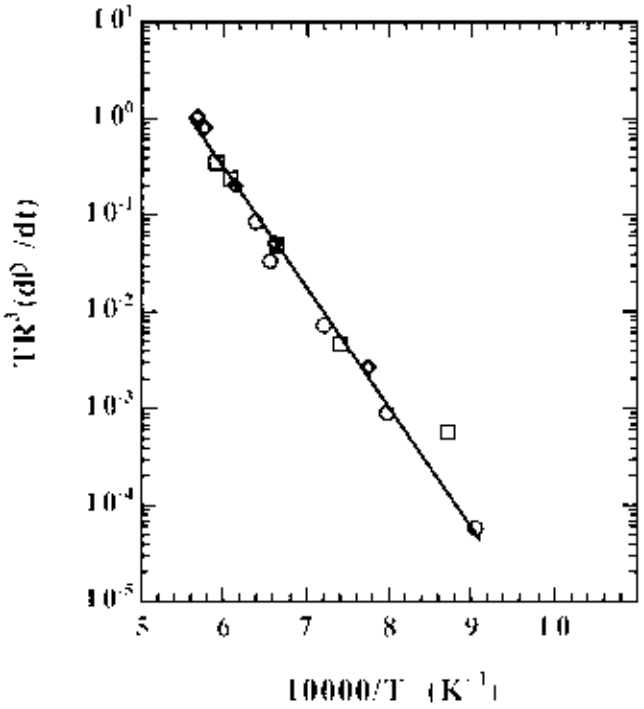

Fig. 11. Size-compensated densification rate versus reciprocal temperature, with $m = 3$, for Y_2O_3 at various densities ((○) 60%, (□) 70%, and (◇) 84%).

proposed recently,[17,18] can break the particle network loose and render it a ramified, "tree"-line structure, at least locally. Because coarsening of the "branches" does little to alter the spatial extent and overall dimension of the network, very little densification results on a macroscopic scale. As particles coarsen and some relocation occurs, the ramified microstructure gradually homogenizes and more particle–particle contacts are established, as discussed in Paper I. Eventually, the particle network approaches that of a homogeneous network with a narrower pore-size distribution. This, in turn, allows coordinated particle movement, depicted in Fig. 6, to occur and the propagation of the displaced pore space to the outer boundary of a macroscopic body to proceed without being disrupted by low-connectivity "weak links." At this point, the transition between regions I and II is complete.

We may now delineate the three sintering regions and the sequence of events by referring to Fig. 6 of Paper I and Fig. 5 in this paper, schematically replotted in Fig. 13. The main process in region I is that of homogenization and stochastic particle relocation. Coarsening at this stage is correlated to homogenization and relocation but not densification. The r/R ratio in this region rapidly converges toward the universal curve given by Eq. (2) of Paper I. The main process in region II is repacking. Densification proceeds by particle repacking, which is motivated by coarsening, and their kinetics are both related to surface diffusion. This continues until $\rho = \rho_{rcp}$, beyond which no particle rearrangement is allowed. Densification in region III is controlled by vacancy transport through grain-boundary or lattice diffusion, which is indirectly affected by particle coarsening by way of diffusion distance.

IV. Discussion

(1) Analogy with Liquid-Phase Sintering

The central part of our analysis, complementing the idea of stochastic particle relocation and homogeneous particle network of Paper I, is captured in the image of coordinated particle movement that achieves densification by repacking. Such a model is admittedly simplistic, considering the many types of particle rearrangement (e.g., a large pore may be dissociated into two smaller pores), the continuous distribution of particle size and pore size, the presence of particle agglomerates and aggregates, and the operation of the conventional sintering mechanisms that must coexist to various extents in "real" sintering. Nevertheless, it is offered to illustrate a new mechanism that explains why low-density compacts densify, despite sometimes having a majority of pores exceeding the critical size. In

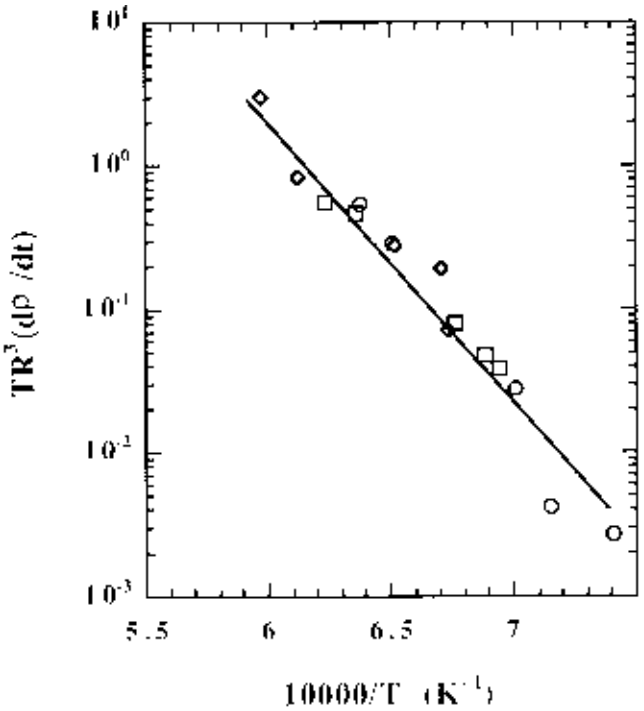

Fig. 12. Size-compensated densification rate versus reciprocal temperature, with $m = 3$, for CeO_2 at various densities ((○) 60%, (□) 70%, and (◇) 84%).

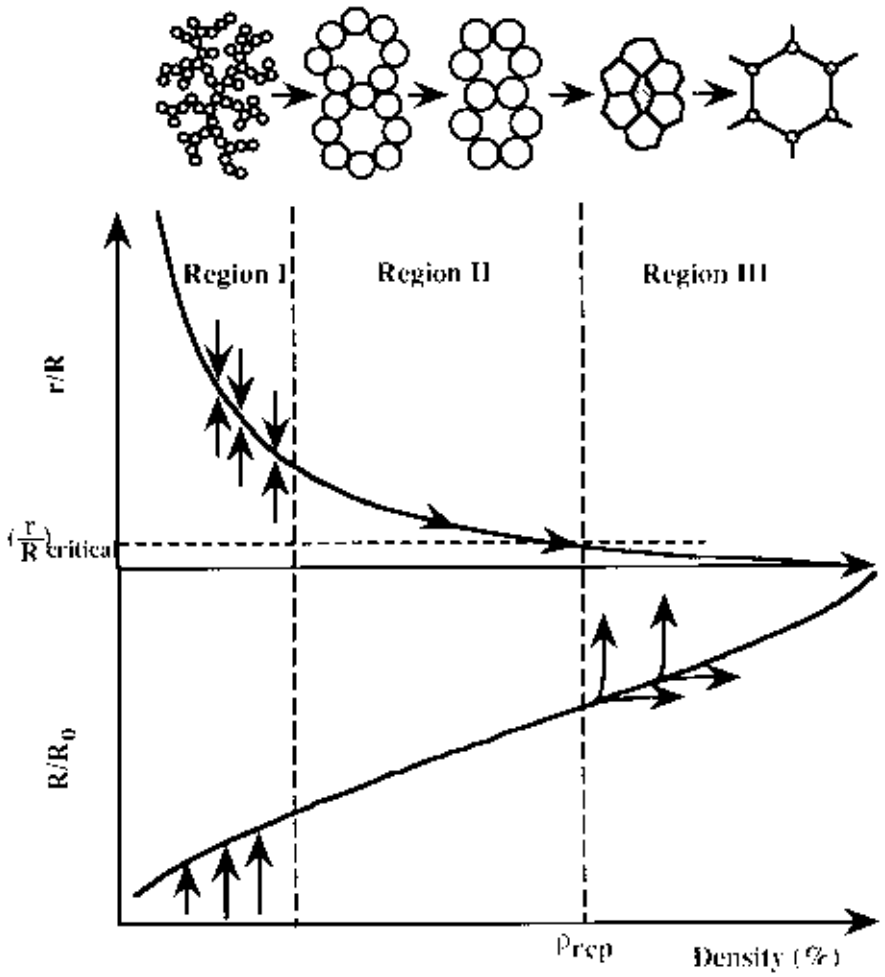

Fig. 13. Schematic diagram for various sintering stages. Pores in region III are shaded.

retrospect, our idea of densification by particle rearrangement rather than by vacancy diffusion is analogous to that of Kingery[19] for the initial stage of liquid-phase sintering. Both mechanisms recognize that much densification can be achieved by improving the packing factor, all the way to random close packing, without shape deformation of the particles. Only after repacking is completed does shape deformation of particles become necessary, and mass transport via lattice diffusion, grain-boundary diffusion, or solution–reprecipitation (as in the case of liquid-phase sintering) become rate limiting. By assuming particle coarsening, grain sliding, and grain rotation, our model envisioned in Fig. 6 allows solid-state sintering to also take advantage of this repacking mechanism, just as the presence of a wetting liquid provides the motivation and means for particle repacking in liquid-phase sintering. Because, geometrically speaking, this repacking mechanism offers the most effective way to achieve densification, it should be the dominating mechanism in fine powders until it is geometrically exhausted (as when $\rho > \rho_{rcp}$) or when the coupling between the local length scale and the macroscopic length scale is disrupted (as with a low-connectivity particle network in some low-density compacts).

(2) Particle-Size Distribution

An interesting issue concerning the present mechanism is whether particles can grow in size without building necks between them. We believe this would be possible if particles are not all the same size and if some grow by incorporating their smaller neighbors. (Indeed, if particles are all the same size, then even in the simplified picture of Fig. 6, the initial eight-particle ring is energetically stable. This is because they are located at a local energy minimum; hence, no coarsening should occur for an indefinite time until a larger perturbation is present.) This scenario has been depicted by Greskovich and Lay[3] and involves some initial neck filling between a large particle and a small particle, followed by rapid grain-boundary migration that sweeps across the smaller particle. Therefore, if one of the initial eight particles in Fig. 6 is considerably smaller than its neighbors, and if it is in contact with a particle that is somewhat larger than the remaining six particles, then the disappearance of the smallest particle and the growth of the largest particle conceivably can be completed without appreciable neck filling between all other particles. Then, a coordinated, inward movement of the remaining seven particles can still happen, and the pore space can still be displaced outside the initial ring of eight particles. Thus, a certain particle-size distribution is probably sufficient to initiate the evolution of network microstructure in any powder compact and is required to facilitate the sequence of events ideally depicted in Fig. 6.

(3) Other Coarsening Mechanisms in Low-Density Compacts

We have identified a nondensifying coarsening mechanism in this work. Contrary to the conventional wisdom in the sintering field, such coarsening is beneficial and is a central element of the homogenization process as well as being a prelude to the densification mechanism. In the literature, another nondensifying coarsening mechanism exists that has been extensively studied using vapor-phase-transfer conditions. As demonstrated by Bheemineni and Readey,[20] coarsening can be greatly enhanced if vapor-phase transport is promoted—typically with a special gas atmosphere. The particle-size distribution in this case has been shown to coarsen in a self-similar manner, indicating a steady-state evolution. However, sintering in this case seems to

be permanently suppressed, unlike the case in our experiment in which coarsening is always followed by densification at a certain stage. We believe the coarsening path in this case is fundamentally different from that observed in our experiment, in that vapor-phase transport allows long-range material deposition without necessarily redistributing their mass to neighboring particles. Perhaps even more significant is the tendency to form highly developed necks between particles by vapor transport, which has the consequence of greatly increasing the network rigidity that prevents particles from rearranging. Therefore, in this case, densification cannot proceed via the mechanism depicted in Fig. 6, whereas the kinetics for the conventional solid-state sintering mechanisms have been largely reduced because of the coarsened microstructure. Thus, although such a coarsening mechanism is possibly beneficial as a homogenization process, it is not conducive to densification.

(4) Attributes of Fine Powders

We have seen from the above analysis that particle coarsening is essential in microstructure evolution and in the densification of fine powder compacts. To reflect on the unique features of the sintering of very fine powders, we see an important distinction between powders that coarsen and those that do not coarsen. For powders that do not coarsen (e.g., larger size or lower surface diffusivity), the initial packing density must be sufficiently high, preferably $>\rho_{rcp}$, to ensure sinterability. (Slightly lower density is acceptable when a large dihedral angle and uniform packing are achievable, both ensuring a pore size that is subcritical.) Sintering in this case is via the conventional sintering mechanisms, and particle coarsening may be avoided until very high densities.[7,8] For powders that coarsen readily (e.g., smaller size or higher surface diffusivity), sintering their compacts at much lower density is possible. Sintering, in this case, is initially by coarsening-motivated repacking of particles until ρ_{rcp} is attained, beyond which solid-state sintering is again active. Although nondensifying coarsening may be encountered initially, continuous coarsening will eventually render coordinated repacking possible and packing density improved, provided the particle network remains flexible enough, which seems to be the case in the fine powder compacts investigated in this study. Thus, the advantage of very fine, highly active powders is directly related to their ability to coarsen, and that improved sinterability is necessarily accompanied by a greatly coarsened microstructure when the common heating schedule for ceramic sintering is followed.

V. Conclusions

(1) Conventional sintering models are applicable at $\rho > \rho_{rcp}$ when essentially all pores are subcritical. Herring's scaling law has been verified in CeO_2 and Y_2O_3 in the density range of 60%–84%; its kinetics are apparently controlled by grain-boundary diffusion.

(2) Particle repacking is allowed at $\rho < \rho_{rcp}$ in fine powder compacts where many pores are supercritical and thermodynamically stable but the particle network is still flexible. By maintaining particle–particle contacts and conserving mass, particle coarsening can lead to coordinated particle movement, pore-volume decrease, and packing-density increase, regardless of the normalized pore size and density.

(3) In poorly packed compacts, coarsening is initially ineffective in motivating densification because of poor particle connectivity, which disrupts particle movement and pore-space redistribution. Particle relocation is mostly stochastic, which, in time, homogenizes the pore-size distribution and disintegrates the very large pores without overall shrinkage on a macroscopic scale.

(4) Very fine, surface-active powders that coarsen rapidly are uniquely capable of taking advantage of coarsening-motivated homogenization and rearrangement densification processes. This accounts for their remarkable sinterability, even at very low green densities.

References

[1]P.-L. Chen and I-W. Chen, "Sintering of Fine Oxide Powders: I, Microstructural Evolution," *J. Am. Ceram. Soc.*, **79** [12] 3129–41 (1996).

[2]Y. Moriyoshi and W. Komatsu, "Kinetics of Initial Sintering with Grain Growth," *J. Am. Ceram. Soc.*, **53** [12] 671–75 (1970).

[3]C. Greskovich and K. W. Lay, "Grain Growth in Very Porous Al_2O_3 Compacts," *J. Am. Ceram. Soc.*, **55** [3] 142–46 (1972).

[4]T. K. Gupta, "Possible Correlation Between Density and Grain Size During Sintering," *J. Am. Ceram. Soc.*, **55** [5] 276–77 (1972).

[5]J. H. Rosolowski and C. Greskovich, "Theory of the Dependence of Densification on Grain Growth During Intermediate-Stage Sintering," *J. Am. Ceram. Soc.*, **58** [5–6] 177–82 (1975).

[6]J. A. Varela, O. J. Whittemore, and M. J. Ball, "Structural Evolution During the Sintering of SnO_2 and SnO_2–2 mol% CuO"; pp. 259–68 in *Sintering '85*. Edited by G. C. Kuczynski, D. P. Uskokovic, H. Palmour III, and M. M. Ristic. Plenum, New York, 1985.

[7]C. P. Cameron and R. Raj, "Grain Growth Transition During Sintering of Colloidally Prepared Alumina Powder Compacts," *J. Am. Ceram. Soc.*, **71** [12] 1031–35 (1988).

[8]T. S. Yeh and M. D. Sacks, "Effect of Green Microstructure on Sintering of Alumina"; pp. 309–31 in Ceramic Transactions, Vol. 7, *Sintering of Advanced Ceramics*. Edited by C. A. Handwerker, J. E. Blendell, and W. A. Kaysser. American Ceramic Society, Westerville, OH, 1988.

[9]R. J. Brook, "Controlled Grain Growth"; pp. 331–64 in *Treatise on Materials Science and Technology, Vol. 9*. Edited by F. F. Y. Wang. Academic Press, New York, 1976.

[10]G. L. Messing and M. Kumagai, "Low-Temperature Sintering of α-Alumina-Seeded Boehmite Gels," *Am. Ceram. Soc. Bull.*, **73** [10] 88–91 (1994).

[11]W. D. Kingery and B. Francois, "The Sintering of Crystalline Oxides: I. Interactions Between Grain Boundaries and Pores"; pp. 471–96 in *Sintering and Related Phenomena*. Edited by G. C. Kuczynski, N. A. Hooton, and C. F. Gibbon. Gordon and Breach, New York, 1967.

[12]W. D. Kingery and M. Berg, "Study of the Initial Stages of Sintering Solids by Viscous Flow, Evaporation–Condensation, and Self-Diffusion," *J. Appl. Phys.*, **26** [10] 1205–12 (1955).

[13]T. Egami and S. Aur, "Local Atomic Structure of Amorphous and Crystalline Alloys: Computer Simulation," *J. Non-Cryst. Solids*, **89**, 60–74 (1987).

[14]P.-L. Chen and I-W. Chen, "Grain Boundary Mobility in Y_2O_3: Defect Mechanism and Dopant Effects," *J. Am. Ceram. Soc.*, **79** [7] 1801–809 (1996).

[15]P.-L. Chen and I-W. Chen, "The Role of Defect Interaction in Boundary Mobility and Cation Diffusivity of CeO_2," *J. Am. Ceram. Soc.*, **77** [9] 2289–97 (1994).

[16]J. D. Hansen, R. P. Rusin, M. H. Teng, and D. L. Johnson, "Combined-Stage Sintering Model," *J. Am. Ceram. Soc.*, **75** [5] 1129–35 (1992).

[17]F. F. Lange and B. J. Kellett, "Thermodynamics of Densification: II, Grain Growth in Porous Compacts and Relation to Densification," *J. Am. Ceram. Soc.*, **72** [5] 735–41 (1989).

[18]R. M. Cannon and W. C. Carter, "Interplay of Sintering Microstructures, Driving Forces, and Mass Transport Mechanisms," *J. Am. Ceram. Soc.*, **72** [8] 1550–55 (1989).

[19]W. D. Kingery, "Densification During Sintering in the Presence of a Liquid Phase: I. Theory," *J. Appl. Phys.*, **30**, 301–306 (1959).

[20]V. Bheemineni and D. W. Readey, "Vaporization of Magnesium Oxide in Hydrogen"; pp. 553–61 in Advances in Ceramics, Vol. 10, *Structure and Properties of MgO and Al_2O_3 Ceramics*. Edited by W. D. Kingery. American Ceramic Society, Columbus, OH, 1984. □